ELSEVIER

Journal of Electron Spectroscopy and Related Phenomena 107 (2000) 261–271

JOURNAL OF ELECTRON SPECTROSCOPY and Related Phenomena

www.elsevier.nl/locate/elspec

Orbital mapping of carbon thin films by XANES-spectromicroscopy

C. Ziethen[a,*], O. Schmidt[a], G.K.L. Marx[a], G. Schönhense[a], R. Frömter[b], J. Gilles[b], J. Kirschner[b], C.M. Schneider[c], O. Gröning[d]

[a] *Johannes Gutenberg-Universität, Institut für Physik, D-55099 Mainz, Germany*
[b] *Max-Planck-Institut für Mikrostrukturphysik, D-06120 Halle, Germany*
[c] *Institut für Festkörper-u. Werkstofforschung, D-01171 Dresden, Germany*
[d] *Universität Fribourg, Institut für Physik, CH-1700 Fribourg, Switzerland*

Received 4 October 1999; received in revised form 13 March 2000; accepted 5 April 2000

Abstract

A laterally resolved micro-XANES study (X-ray absorption near edge structure) of amorphous carbon, hydrogen terminated CVD-diamond (100) and highly oriented pyrolytic graphite (HOPG) is presented. The results were obtained by means of a photoemission electron microscope. Using this technique the well-known spectral features of carbon in its different chemical states (sp^2, sp^3) could be recorded. The sp^2/sp^3 content of the films was extracted from the spectra. Images, taken at X-ray energies corresponding to maxima (π^*, C–H*) of the unoccupied density of states in these spectra, map the lateral distribution of the different orbitals at the sample surface. This study revealed graphitic areas on a well-ordered diamond surface and shows the location of C–H bonds on edges of the basal plane of the HOPG. Profiting from the elemental selectivity of the method, even weak traces of iron contaminations are mapped at the diamond surface.

Keywords: Spectromicroscopy; X-PEEM; μ-XANES; Orbital mapping; Diamond; Amorphous carbon; Graphite

1. Introduction

Diamond and diamond like thin films have been of growing interest in the last years. This is because of their outstanding physical, chemical and mechanical properties. They bear a high technical potential and are often used by engineers as a wear-resistant coating of surfaces. Owing to their very high hardness, the lifetime of coated tools can be increased significantly. For the chemical and structural characterization of carbon thin films site selective techniques are mainly used which are capable to differentiate between sp^2 and sp^3 hybridized carbon (graphite, diamond). In particular, these are XANES (X-ray absorption near edge structure) spectroscopy [1–9], EELS (electron energy loss spectroscopy) [10,11], inverse-photoemission spectroscopy and tunneling spectroscopy [12], SXAPS (soft X-ray appearance potential spectroscopy) and BIS (Bremsstrahlung isochromat spectroscopy) [13], all probing the differences in the unoccupied density of states (UDOS). Other techniques are Raman spectroscopy [9,14,15], spectroscopic ellipsometry [16,17], UPS and XPS (ultraviolet/X-ray photoemission spectroscopy) and AES (Auger electron spectroscopy) [14,18]

In order to image the structure, especially of

*Corresponding author. Fax: +49-613-1-3923807.
E-mail address: ziethen@mail.uni-mainz.de (C. Ziethen)

0368-2048/00/$ – see front matter
PII: S0368-2048(00)00151-1

diamond films with high lateral resolution, results have been obtained using scanning electron microscopy (SEM) [15] and atomic force microscopy (AFM) [18]. In the latter study, a combination of UPS/XPS, AES, XANES, Raman spectroscopy and AFM was applied to shed light on the nucleation and growth of diamond films. For the still open questions on this matter, Simons et al. [18] hoped that XANES microscopy will have the answer. This technique combines XANES spectroscopy with a photoemission electron microscope to 'XANES-spectromicroscopy', providing sensitivity for chemical elements and differences in the chemical environment of the absorbing atom with high lateral resolution. A review of the current status of this rather new characterization technique was published previously [19].

In the present paper, the applicability of XANES-spectromicroscopy to investigate problems of diamond and diamond-like films is proven. Using a photoemission electron microscope (PEEM), we have recorded orbital maps at the carbon K-edge of 'diamond-like' amorphous carbon (a-C), highly oriented pyrolytic graphite (HOPG), and CVD-diamond (100) films grown on silicon. Because of the remarkable differences of the carbon K-shell near edge structures, we were able to distinguish the different hybridization states of carbon. Thus, graphitic areas on diamond films, selective hydrogen adsorption on defects, as well as contaminations (Fe), could be detected with high sensitivity and lateral resolution.

2. Experimental

2.1. Technical features of the PEEM

In our experiments, we use a compact and versatile photoemission microscope (FOCUS IS-PEEM) [20]. The sample is illuminated by the soft-X-rays coming from a tunable monochromator at the storage ring BESSY GmbH, Berlin (monochromator PM3 of the SX700 type) at a bending magnet beamline. The secondary electrons which are generated in the sample are collected and accelerated by a high electrostatic field (5–8 kV mm^{-1}) between the sample and the first electrode of the immersion objective lens. After magnification by a two-stage projective lens system and intensification via a multichannel-plate, the lateral distribution of electrons is made visible on a YAG single crystal luminescent screen. Using an integrated, piezomotor driven x/y sample mount, the specimen can be shifted by ± 2.5 mm in x and y direction. The lateral resolution of the microscope is mainly determined by the extractor voltage, the energy of the incoming light and the diameter of the aperture located in the back focal plane of the objective lens. The aperture can be changed and adjusted during operation with five different sizes ranging from 1500 down to 30 μm. The lateral resolution reached is 130 nm at $h\nu = 540$ eV (synchrotron radiation) and better than 20 nm at $h\nu = 4.9$ eV (mercury lamp) [21]. The probing depth for 3d-transition metals lies in the range of 3 nm, as has been measured by evaluating monolayer steps of evaporated Cr on an iron whisker [22] and corresponding to the results of Stöhr et al. [43]. It is mainly determined by the mean free path of the inelastically scattered secondary electrons. X-PEEM is thus a very surface sensitive technique. Using peltier cooled slow-scan CCD-cameras, we have recorded images of the surface area with the field of view varying between 0.8 mm and 10 μm. More results, showing the versatility of the microscope used, are μ-ESCA (electron spectroscopy for chemical analysis) [23], time-of-flight (TOF) spectroscopy [24], and magnetic domain imaging [22,25].

2.2. Laterally resolved XANES spectroscopy

A CCD video-camera has been used for recording the μ-XANES spectra at grazing light incidence (25°). With this camera system, we defined up to ten regions of interest in the microscope image. Depending on the intensity, the size of the measuring spot can be decreased down to the sub-micron range. For a test sample (Pd stripes on Si substrate), a value of 500×500 nm^2 has been reached. While tuning the X-ray energy of the monochromator (typical step-width 0.25 eV, energy range 50–1500 eV at the PM3), the intensity plots of all defined areas are recorded simultaneously. The energy resolution is 1900 at $h\nu = 707$ eV [26]. Because of the fact that the image intensity of the spots depends linearly on the yield of the secondary electrons coming from the

corresponding sample area, one can directly obtain the so called partial electron yield (PEY) μ-XANES spectra. This is due to the fact, that the electron yield is directly proportional to the X-ray absorption, as has been reported by Gudat and Kunz [27], but the microscope acts as a low-pass filter for high energy electrons [28,29]. Fig. 1 illustrates the basic principle of chemical contrast formation.

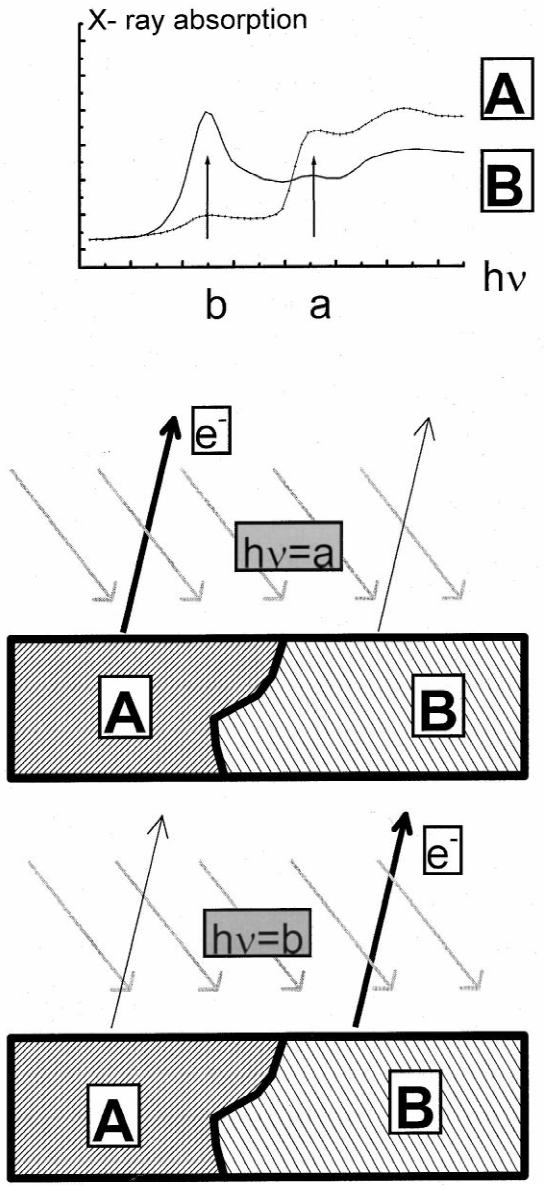

Fig. 1. Principle of photoabsorption spectromicroscopy. μ-XANES spectra from sample position A and B show distinct differences.

For a quantitative comparison of the results with previous non laterally resolved data in the literature, the spectra have to be calibrated for the energy dependent monochromator transmission, which is characterized by strong absorption features at the carbon K-edge, the O K-edge and the Cr L-edges. This was done by normalizing the data with calibration spectra collected from the surface of a silicon wafer and a gold film. The energy scale of the spectra was calibrated in two ways. Because the diamond and graphite show three resonances (π*, C–H*, gap of the diamond band structure) at characteristic energies and both samples were measured at the same time in the field of view of the microscope, we used these energies for calibrating the monochromator in the XANES energy range. In order to confirm this, we used a wide range calibration spectrum, determined the energetic position of the C-, O- and Cr-absorption features and compared them with the energies reported in the literature.

3. Results and discussion

3.1. Amorphous carbon

Our first test of the method was the examination of a piece of silicon wafer, covered by an 6×6 mm^2 area of an unknown material, which was so hard that it could not be scratched by steel. We supposed, the film to be diamond-like and tried to prove it by μ-XANES.

Fig. 2a shows an image obtained at the border of the carbon film. The excitation source was a mercury high pressure lamp ($h\nu=4.9$ eV), so the image intensity is mainly determined by differences in the workfunction. The image diameter was 500 μm approximately. The irregularly shaped surface area A consists of dried Aquadag (colloidal carbon) deposited for comparison. It is expected to exhibit amorphous spectral characteristics [12]. Area B corresponds to the very hard film, area C to a soft carbon film and area D shows the underlying silicon wafer. Before examination, the sample temperature was increased for 2 min to red heat for cleaning the surface.

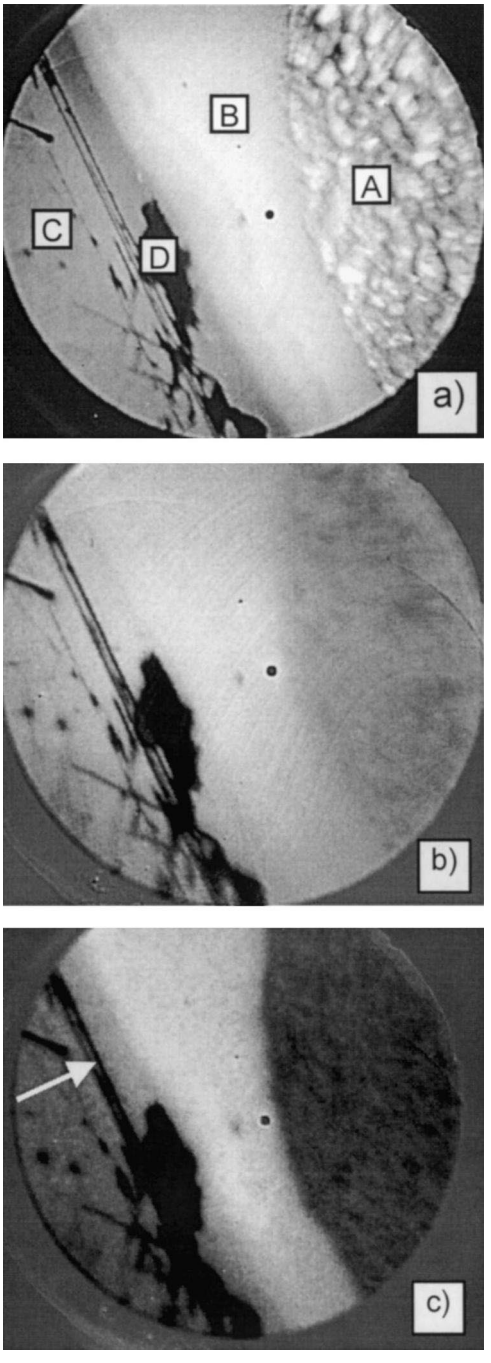

Fig. 2. Images of the carbon sample. (a) $h\nu = 4.9$ eV (mercury lamp), (b) distribution of amorphous carbon a-C (taken at $h\nu = 285$ eV), (c) distribution of a-C with high content of sp^3-coordinated atoms (taken at $h\nu = 292$ eV). The field of view is 500 μm, integration time was 5 s for (a) and 120 s for (b) and (c); the squares mark the regions for the μ-XANES spectra in Fig. 3.

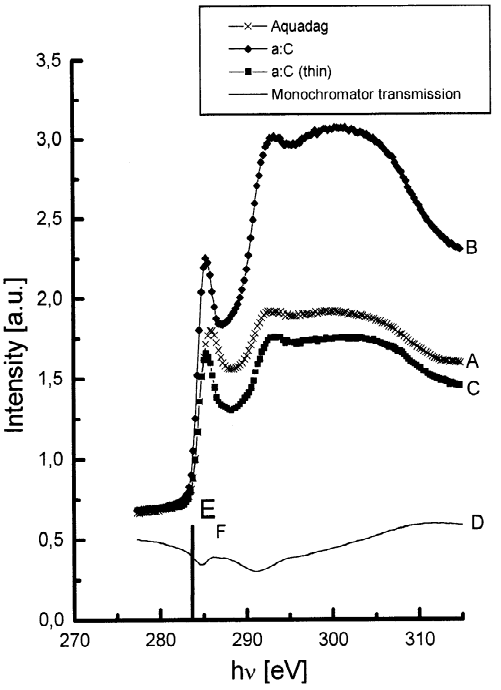

Fig. 3. μ-XANES spectra of amorphous carbon a-C, obtained at positions A–C (see Fig. 2). D shows the monochromator transmission. Spectra A–C are normalized by spectrum D.

Fig. 3 shows carbon K-edge μ-XANES spectra at the regions of interest A–D as defined in Fig. 2a. In the spectra A–C the typical absorption edges and near edge structures of amorphous carbon [6–9] appear. The $1s \rightarrow \pi^*$ transition ($h\nu = 285.3$ eV at B and C, 286 eV at A) is the most prominent feature of sp^2 coordinated graphitic carbon, as observed by EELS [10], XAS [2,3,8,9,30], inverse photoemission and tunneling spectroscopy [12]. Here, we assigned it to carbon atoms with graphitic short range order in an amorphous matrix. It is remarkable, that at the position D no carbon signal, but two absorption minima are detected, resulting from the monochromator transmission. This is due to the fact, that the carbon layer has peeled off there and the underlying silicon wafer is visible. We normalized the spectra A to C by spectra D for correction of the intensity scale. The almost featureless part at energies higher than ≈292 eV is dominated by transitions to σ^* bands and shows only two broad maxima around 292 and 301 eV.

The intensity ratio of the areas of the π^* peak

(integrated between 282.1 and 287.4 eV) and the rest of the spectrum (integrated between 287.4 and 320.1 eV) is used for determining the sp^2 (graphite-like) content of the carbon films [31]. It has the value 0.075 at the position B on the hard a-C film, which is 25% lower than those values measured on the carbon layer on top of the silicon (0.095, position C) and on the Aquadag (0.101, position A). The reason for the very high hardness of the hard a-C coating, compared to the softer one and the Aquadag is clearly this decrease in sp^2 and the increase in the sp^3 (diamond-like) bonding contribution. The absolute value of the sp^2 and sp^3 content is obtained, if these intensity ratios are normalized with the ratio of graphite, which is believed to have a 100% sp^2 content (see Section 3.2.). Note, that these values correspond to the probing depth of about 3–5 nm.

One of the benefits of our method is the possibility to map the elemental distribution and the density of states at the sample surface. This is facilitated by taking an image at the energy of a distinct core level or orbital and subtracting the corresponding background image obtained at an X-ray energy a few eV lower. Fig. 2b shows the distribution of carbon at the sample surface by mapping the π^* orbital. The area which remains dark is the silicon wafer, where the carbon layer has come off. The distribution of the a-C hard film with higher sp^3 content is shown in Fig. 2c as a bright area. In contrast, in this image the Aquadag appears dark and the soft a-C in an intermediate grey level. Note, that the hard a-C film extends to two dark lines, marked by an arrow. This is well beyond the border of the film as estimated from the image dominated by workfunction contrast in Fig. 2.

3.2. Graphite and diamond (100)

Further μ-XANES spectra have been taken of an artificial diamond film with (100)-oriented crystallites and HOPG (Advanced Ceramics).

The diamond film was grown in a microwave plasma. Hydrogen pressure was 40 mbar with 1% CH_4. Subsequently it was treated in a ECR (electron cyclotron resonance) plasma for 120 min at 10^{-2} mbar H_2 for saturating the dangling bonds. The film thickness was 7 μm, the size of the irregularly shaped diamond crystallites was approximately 2 μm as measured by SEM (scanning electron microscopy). For the experiment a sample was prepared which contained two distinct areas, one with the diamond film and the other one with the HOPG. So the spectra of the diamond film and the HOPG could be recorded simultaneously. No heating or cleaning by ion sputtering was applied in order to avoid the sample to get amorphous or to remove the hydrogen from the surface.

Data collection time for the spectra was 2.6 s per point, the stepwidth of the monochromator was set to 0.25 eV. The size of the selected microspots are 20×20 μm^2 on featureless areas and about 5×5 μm^2 on distinct details. The microspectra, normalized to the monochromator transmission are shown in Fig. 4. Well known spectral features typical for graphite and diamond [5,9,32–35] are marked by arrows. The first peak is the most prominent fingerprint-like spectral feature of sp^2-coordinated carbon in graphite ($1s\rightarrow\pi^*$ transition at 284.8 ± 1.6 eV). It is

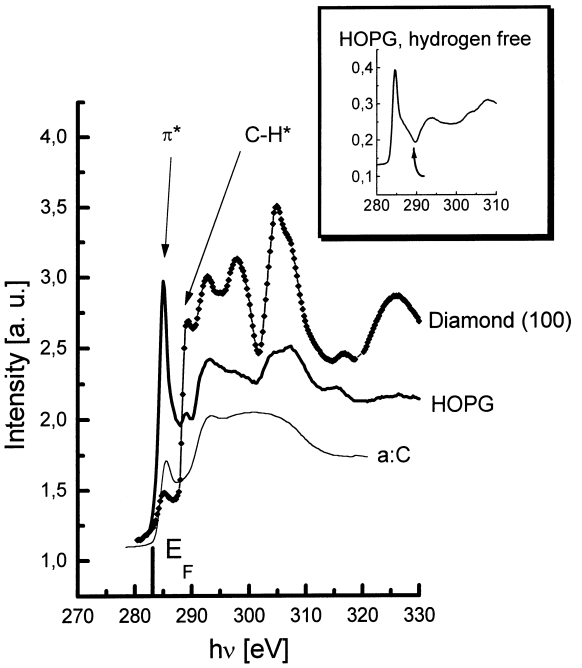

Fig. 4. μ-XANES spectra of the diamond (100) film and HOPG, both treated in a hydrogen plasma and recorded in 5×5 μm^2 microspots. An a-C spectrum is shown for comparison. The inset shows the μ-XANES spectrum of a 20×20 μm^2 area outside the field of view in an undistorted region of the same sample. It is hydrogen free and shows no C–H* peak (curved arrow).

associated with the unoccupied π states of the conduction band around the Q [2], M and L [36] points of the Brillouin zone. It is nearly dispersionless at 2 eV above E_F along the M–L line. Because the bandstructure of graphite is nearly two dimensional, this gives a sharp Van-Hove type contribution to the UDOS (Unoccupied density of states).

Due to the fact that the intensity of the 1s–π* transition depends on the angle of photon-incidence, we recorded the HOPG spectrum at a position at the sample surface, which looks disordered. This justifies the assumption that the nanoscopic structure is disordered as well, and that is why angle-dependent effects will be canceled by averaging.

The second prominent feature in Fig. 4 can be assigned to the C–H* resonance (at 289.2 eV), which is typical for sp^3 coordinated carbon with a high content of hydrogen [5]. It appears nearly at the same energy, where a core-hole excitonic state is observed in natural diamond [37], artificial diamond and graphitic materials [9] and in hydrogen-free amorphous carbon films [38]. The exciton appears, if the short range order is good. In the case of diamond, the π* peak vanishes (see the results published by Coffman et al. [9]). In our case, where a clear π* peak is observed, no remarkable contribution of the excitonic state is expected. By comparing the diamond spectrum with the HOPG spectrum, we note, that the latter shows a small peak at the photon energy of the diamond C–H* transition. On the other hand, a HOPG spectrum recorded at a structureless flat sample position outside the images of Fig. 5 shows no peak at this energy (inset in Fig. 4). To get a close up view of what happens, Fig. 5a shows the lateral distribution of the π* orbital corresponding to the HOPG. The diamond surface at top remains dark. Fig. 5b represents the lateral distribution of the orbital corresponding to the C–H* resonance. Now, the graphite surface remains dark. Contrast enhancing of Fig. 5b leads to the image in Fig. 5c, where the diamond is completely overmodulated, but the HOPG shows distinct details now. Further we acquired a second image with higher magnification (Fig. 5d), which shows one of the areas, where the HOPG spectra with C–H* peak have been recorded. Especially the curved kinks or atomic step bunches on the HOPG appear brighter in the light of the C–H* orbital. The expected multiple atomic steps which are part of the kinks, are unresolved at this resolution and the corresponding intensity coming from the C–H* bondings is the integral over the marked area. The kinks obviously exhibit dangling bonds saturated by hydrogen during the ECR plasma treatment. In the image of the same region, obtained with a mercury lamp (Fig. 5e), those areas which show higher intensity at the C–H* resonance, are remarkably brighter due to a lower workfunction.

Our results give a useful contribution to the discussion concerning the origin of this spectral feature in the graphite UDOS [5]. In inverse photoemission and tunneling spectra of graphite [12], this feature was observed at an energy of $h\nu = 3.5$ eV above E_F and assigned to a free-electron-like interlayer band of the graphite [36,39,40]. In graphite single crystals (expected to be hydrogen-free), however, there are no spectral features in the energy range between the π* peak and 292 eV [30,41]. Comelli et al. [8] compared a smooth spectral detail at $h\nu = 289$ eV with XANES spectra of benzene and cyclohexane (C_6H_6, C_6H_{12}) and assigned it to hydrocarbon bonds.

The appearance of the C–H* orbital has been studied by Coffman et al. [9] as well. They investigated a series of carbon thin films varying from diamond to graphitic order, examined by XANES and Raman spectroscopy. They show, that with decreasing sp^3 content, the number of unsaturated bonds is increased. This gives a clear C–H* spectral feature for three films, varying from mainly diamond, then amorphous and finally graphitic order.

Our laterally resolved μ-XANES results clearly show that a contribution of C–H* bonds leads to a significant feature at 289 eV in the XANES spectrum of HOPG and that this contribution to the overall shape of a HOPG spectrum results from the existence of the structural defects at the HOPG surface. This result is of particular importance for the interpretation of the XANES spectra of imperfect artificial HOPG or polycrystalline graphite surfaces, grown in an atmosphere containing hydrocarbons and showing steps and defect sites.

3.3. Determination of the sp^2/sp^3 ratio

The ratio of the area of the π* peak and the area of the rest of the spectrum has been determined as

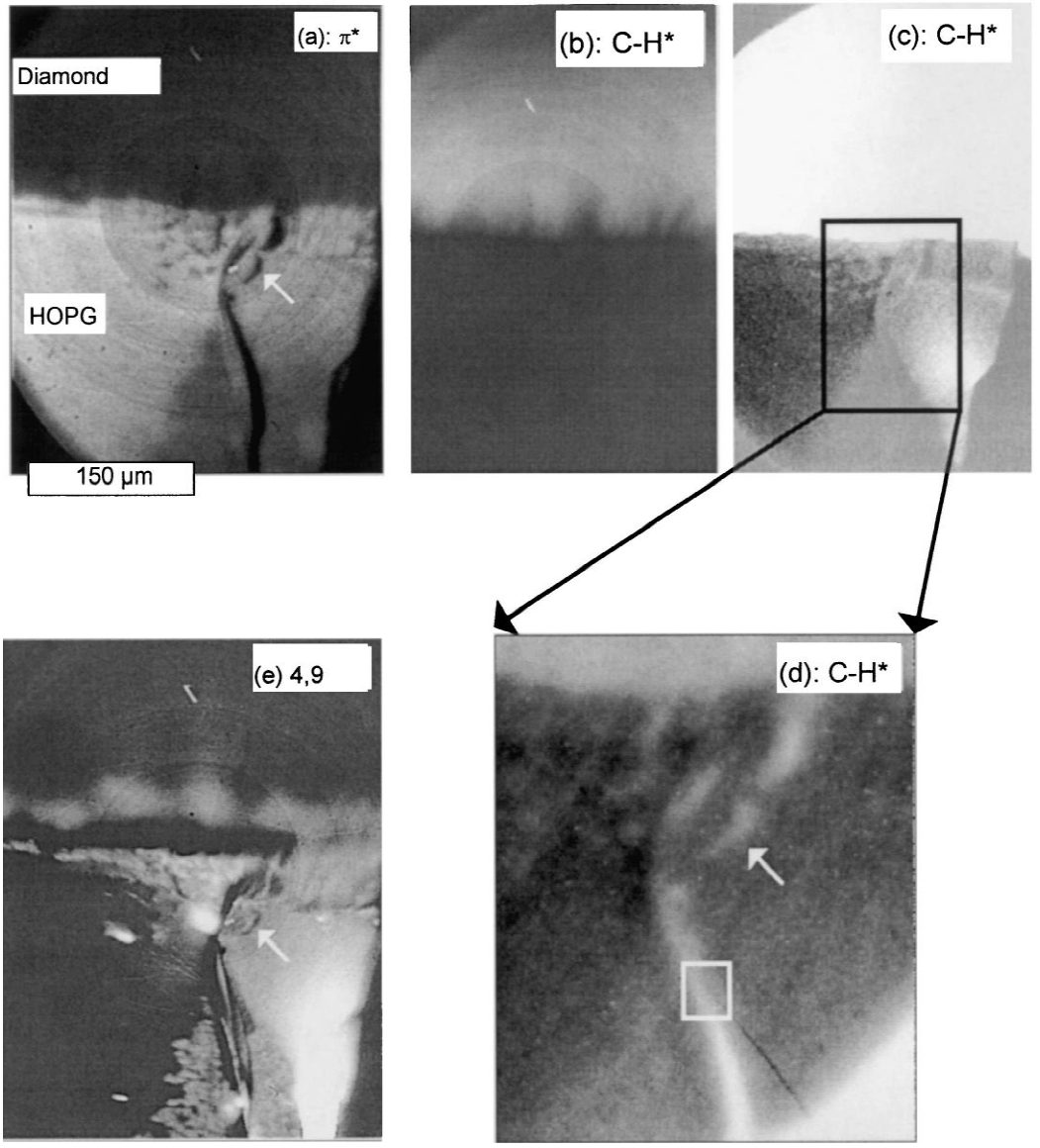

Fig. 5. Lateral distribution of the orbitals π* (a), C–H* (b), C–H* contrast-enhanced (c), close up view of the kinks in the graphite, imaged with the C–H* orbital (d), workfunction contrast obtained using a mercury lamp at $h\nu = 4.9$ eV (e). The radial substructures visible in a, b and e are due to doping inhomogenities in the YAG-screen. The marked area in d is the microspot for recording the HOPG-spectrum in Fig. 4; the three white arrows indicate identical positions. Integration time was 50–60 s for each image.

described in Section 3.1. It is 0.018 on diamond and 0.109 on graphite (compared to 0.075 for hard a-C and 0.095 for soft a-C). The fractions of sp^2 sites in the diamond film and in the amorphous carbon films are derived by normalizing their ratio to that of graphite or Aquadag (results in brackets) According to this calibration, the diamond film has a 16.5% (18%) content of sp^2 sites, the hard a-C 69% (75%) and the soft a-C 87% (95%). These results reflect an uncertainty of $\leq 8\%$ for the determination of the sp^2/sp^3 ratio. The high contribution of graphitic bonds in the diamond is typical for diamond films

grown in a microwave CVD process. Janischowsky and co-workers [44,45] present Raman-spectra of films grown in a microwave plasma, which strongly exhibit amorphous and graphitic contributions to the spectra. The values obtained for a-C are typical, too [8,31]. The result of Comelli et al. is 92±9% for an a-C material with the bonding length of graphite. This corresponds well with our result of 87% for the soft a-C and the 92.5% of Aquadag, both materials can be smeared out with a knife. A figure of 60±6% is given by the authors [8] for typical amorphous carbon comparable with our hard a-C (69%).

3.4. Localized defects at the diamond surface

It was suggested that the origin of the $1s\rightarrow\pi^*$ transition at $h\nu=284.5$ eV of diamond is associated with the C=C bonds or with graphitic contaminations at the surface of the diamond (100) [5]. This leads to the high sp^2 content of the diamond film. Whereas the double bound contribution on an atomic scale is beyond the limits of our experimental method, it might be possible to detect the contribution of isolated graphitic areas in the micron range. In Fig. 6a, the microcrystalline surface of the diamond (100) film is mapped 'in the light' of the C–H* orbital, i.e. at $h\nu=289$ eV. The image reveals many dark patches. By imaging the marked surface area via the π^* orbital, i.e. at $h\nu=286$ three prominent areas are identified as graphitic carbon (Fig. 6b). We have determined the sp^2 content of the diamond surface, varying between 9.5 and 11% across the field of view in Fig. 6a (spectrum A), and 43% in the three 10-μm patches of Fig. 6b (spectrum B). Both spectra show the typical features of diamond, but with a very high π^* peak at position B. So these patches are not contaminations with HOPG, but really diamond with a very high number of sp^2-coordinated carbon atoms. Imaged in the light of the π^* orbital at $h\nu=286$ eV in Fig. 6b, they prominently appear against the weak background of the diamond surface at this photon energy. Grogger et al. [46] have shown that in the nucleation phase of diamond films there can be a tendency to form a-C areas (thickness around 100 nm) on the substrate surface which are then covered by a diamond layer. Our result shows that in this case the sp^2/sp^3 ratio might not reach the grade of a high quality diamond film.

Most of the remaining dark features can be attributed to iron contaminations (Fig. 6c), as has been proven by the appearance of the iron $L_{2,3}$ lines in the spectra (see spectrum C). They cover the surface and are probably caused by contamination during the deposition procedure of the diamond film.

4. Conclusion and outlook

It has been demonstrated that XANES spectromicroscopy represents a unique tool for the quantitative chemical microanalysis of carbon thin films. By combining site selectivity of the XANES spectroscopy with the lateral resolution of the photoemission electron microscope, it was possible to separate the different phases of carbon, to measure the relative sp^2/sp^3 content of carbon films with microscopic resolution and to detect local graphitic phases on diamond thin films by mapping the fingerprint-like π^* orbital. According to our examination of pyrolytic graphite, the existence of graphite interlayer states being excited between $h\nu=285$ and 292 eV seems to be doubtful. Spectral features observed in artificial graphite films can be explained with C–H bonds. The parallel image acquisition of the photoemission microscope in combination with the high brilliance of synchrotron radiation yields short exposure times of the order of several seconds down to the millisecond range for an element-resolved image [47].

The next step into structural microanalysis with our PEEM will be the newly developed version of the microscope, the double reflection emission electron microscope (DREEM) [42]. This instrument gives the possibility to obtain micro-LEED images of the areas examined by μ-XANES, in order to completely evaluate the chemical and structural composition of microscopic sample areas. In the future, μ-XANES/EXAFS/LEED will become a very useful technique not only for the examination of carbon thin films, but also for a wide range of other coatings, some of them containing carbon. Examples are WC, SiC, Cr, CrC, Al_2O_3, C_3N_4–CH_x, $CN_x$with degrees of hardness up to 4500 kp mm^{-2}, very low friction coefficients ($\mu=0.1$–0.25) or very good adhesion on steel. For a combination of these

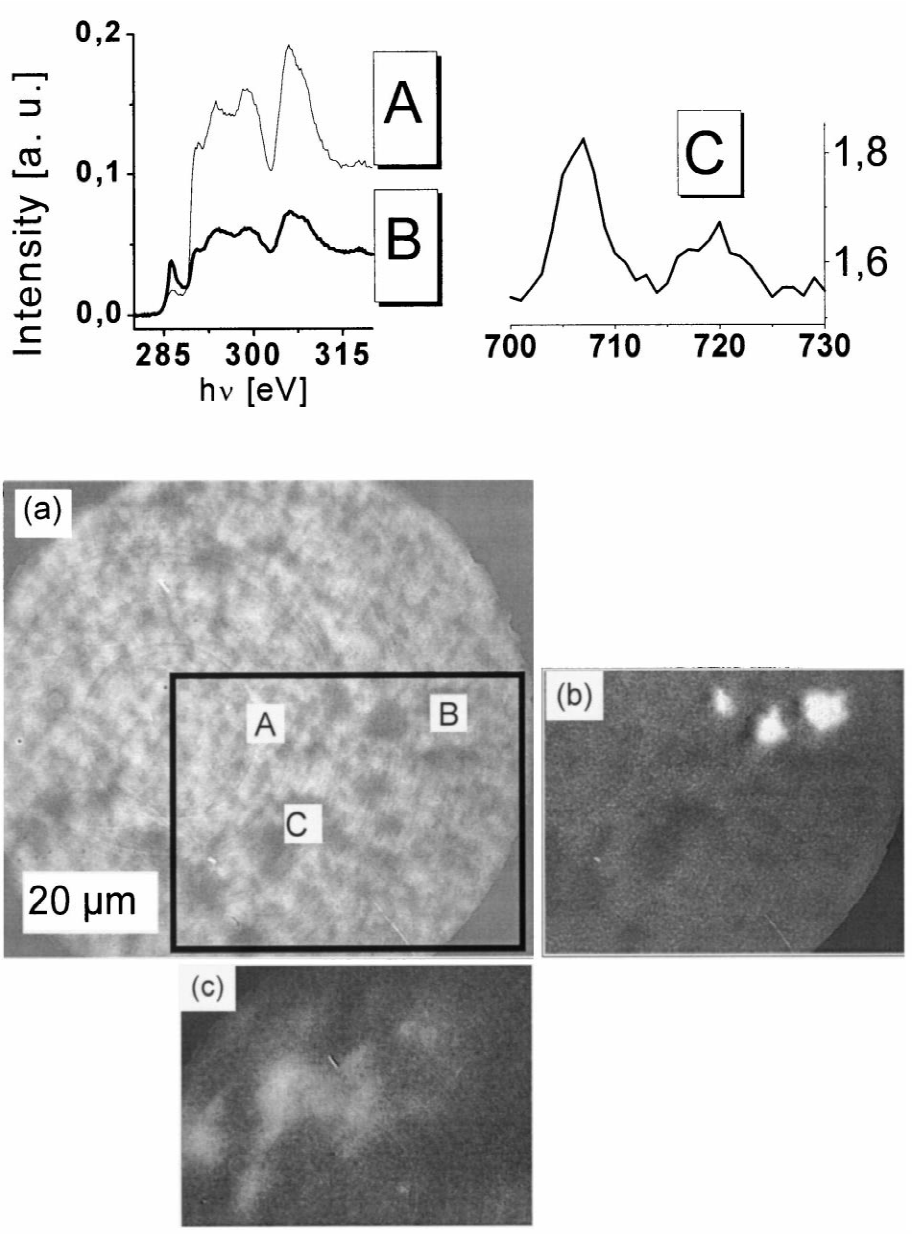

Fig. 6. (a) Lateral distribution of the C–H* orbital on the diamond (100) film surface, (b) three areas of the graphitic phase in the diamond film (π* orbital), (c) traces of iron contamination ($h\nu = 707$ eV, Fe L_{III} edge). A, B and C denote the microspots where the corresponding spectra have been recorded.

properties, nowadays multilayers of these films are in use. Examples are Cr–a-SiC with very good adhesion, low stress and very high hardness (4000 kp mm^{-2}), the WC–Al_2O_3 system which is chemically resistant with a hardness around 3000 kp mm^{-2} and the tribologically favorable film WC–a-C:H. All the chemical elements in these coatings have core levels (K or L edges) in the soft X-ray energy range,

which is easily accessible at most of the synchrotron radiation sources presently running.

Acknowledgements

Thanks are due to the staff of BESSY for fruitful cooperation. The experiment was funded by BMBF through grant No. 05 SC8 UMAO and by Materialwissenschaftliches Forschungszentrum (MWFZ) of the University of Mainz Germany.

References

[1] J. Stöhr (Ed.), NEXAFS Spectroscopy, 1st Edition, Springer Series in Surface Sciences, Vol. 25, Springer, Heidelberg, 1996.
[2] D. Denley, P. Perfetti, R.S. Williams, D.A. Shirley, Phys. Rev. B 21 (1980) 2267.
[3] R.A. Rosenberg, P.J. Love, V. Rehn, Phys. Rev. B 33 (1986) 4034.
[4] J.F. Morar, F.J. Himpsel, G. Hollinger, G. Hughes, J.L. Jordan, Phys. Rev. Lett. 54 (1985) 1960.
[5] Th. Schedel-Niedrig, D. Herein, H. Werner, M. Wohlers, R. Schlögl, G. Francz, P. Kania, P. Oelhafen, C. Wild, Europhys. Lett. 31 (1995) 461.
[6] A. Gutiérrez, J. Díaz, M.F. López, Appl. Phys. A 61 (1995) 111.
[7] A. Gutiérrez, M.F. López, Europhys. Lett. 31 (1995) 299.
[8] G. Comelli, J. Stöhr, C.J. Robinson, W. Jark, Phys. Rev. B 38 (1988) 7511.
[9] F.L. Coffman, R. Cao, P.A. Pianetta, S. Kapoor, M. Kelly, L.J. Terminello, Appl. Phys. Lett. 69 (1996) 568.
[10] B.M. Kincaid, A.E. Meixner, P.M. Platzman, Phys. Rev. Lett. 40 (1978) 1296.
[11] P. Kovarik, E.B.D. Bourdon, R.H. Prince, Phys. Rev. B 48 (1993) 12123.
[12] B. Reihl, J.K. Gimzewski, J.M. Nicholls, E. Tosatti, Phys. Rev. B 33 (1986) 5770.
[13] V. Dose, G. Reusing, H. Scheidt, Phys. Rev. B 26 (1982) 984.
[14] B.S. Elman, M. Shayegan, M.S. Dresselhaus, H. Mazurek, G. Dresselhaus, Phys. Rev. B 25 (1982) 4142.
[15] A.M. Bonnot, Phy. Rev. B 41 (1990) 6040.
[16] S. Logothetidis, J. Petalas, H.M. Polatoglou, D. Fuchs, Phys. Rev. B 46 (1992) 4483.
[17] S. Logothetidis, J. Petalas, S. Boultadakis, I. Alexandrou (Eds.), BESSY Jahresbericht, BESSY, Berlin, 1994, p. 335.
[18] J.K. Simons, R.V. Duevel, S.P. Frigo, J.W. Taylor, R.A. Rosenberg, J. Appl. Phys. 76 (1994) 5481.
[19] H. Ade (Ed.), J. Electron Spectrosc. Relat. Phenom 84 (Special Issue) (1997) 1.
[20] W. Swiech, G.H. Fecher, Ch. Ziethen, O. Schmidt, G. Schönhense, K. Grzelakowski, C.M. Schneider, R. Frömter, H.P. Oepen, J. Kirschner, J. Electron Spectrosc. Relat. Phenom. 84 (1997) 171.
[21] Ch. Ziethen, O. Schmidt, G.H. Fecher, C.M. Schneider, G. Schönhense, R. Frömter, M. Seider, K. Grzelakowski, M. Merkel, D. Funnemann, W. Swiech, H. Gundlach, J. Kirschner, J. Electron Spectrosc. Relat. Phenom. 88–91 (1998) 983.
[22] C.M. Schneider, R. Frömter, Ch. Ziethen, W. Swiech, N.B. Brookes, G. Schönhense, J. Kirschner, Mater. Res. Soc. Symp. Proc. 475 (1997) 381.
[23] O. Schmidt, Ch. Ziethen, G.H. Fecher, M. Merkel, M. Escher, D. Menke, U. Kleineberg, U. Heinzmann, G. Schönhense, J. Electron Spectrosc. Relat. Phenom. 88–91 (1998) 1009.
[24] H. Spiecker, O. Schmidt, Ch. Ziethen, D. Menke, U. Kleineberg, R.C. Ahuja, M. Merkel, U. Heinzmann, G. Schönhense, Nucl. Instrum. Methods A 406 (1998) 499.
[25] W. Kuch, R. Frömter, J. Gilles, D. Hartmann, Ch. Ziethen, C.M. Schneider, G. Schönhense, W. Swiech, J. Kirschner, Surf. Rev. Lett. 5 (6) (1998) 1841.
[26] Ch. Ziethen, PhD thesis, University of Mainz, Shaker, Aachen (1999), ISBN 3-8265-6432-4.
[27] W. Gudat, C. Kunz, Phys. Rev. Lett. 29 (1972) 169.
[28] B.P. Tonner, G.R. Harp, S.F. Koranda, J. Zhang, Rev. Sci. Instrum. 63 (1992) 564.
[29] B.P. Tonner, D. Dunham, T. Droubay, J. Kikuma, J. Denlinger, E. Rotenberg, A. Warwick, J. Electron Spectrosc. Relat. Phenom. 75 (1995) 309.
[30] P.E. Batson, Phys. Rev. B 48 (1993) 2608.
[31] P.J. Fallon, V.S. Veerasamy, C.A. Davis, J. Robertson, G.A.J. Amaratunga, W.I. Milne, J. Koskinen, Phys. Rev. B 48 (1993) 4777.
[32] R.F. Willis, B. Fitton, G.S. Painter, Phys. Rev. B 9 (1974) 1926.
[33] R.C. Tatar, S. Rabii, Phys. Rev. B 25 (1982) 4126.
[34] X. Weng, P. Rez, O.F. Sankey, Phys. Rev. B 40 (1989) 5694.
[35] X. Weng, P. Rez, H. Ma, Phys. Rev. B 40 (1989) 4175.
[36] D.A. Fischer, R.M. Wentzcovitsch, R.G. Carr, A. Continenza, A.J. Freeman, Phys. Rev. B 44 (1991) 1427.
[37] J.F. Morar, F.J. Himpsel, G. Hollinger, G. Hughes, J.L. Jordan, Phys. Rev. Lett. 54 (1985) 1960.
[38] A. Gutiérrez, J. Díaz, M.F. López, Appl. Phys. A 61 (1995) 111.
[39] M. Posternak, A. Baldereschi, A.J. Freeman, E. Wimmer, M. Weinert, Phys. Rev. Lett. 50 (1983) 761.
[40] N.A.W. Holzwarth, S.G. Louie, S. Rabii, Phys. Rev. B 30 (1984) 2219.
[41] R.A. Rosenberg, P.J. Love, V. Rehn, Phys. Rev. B 33 (1986) 4034.
[42] K. Grzelakowski, Rev. Sci. Instrum. 70 (1999) 3346.
[43] J. Stöhr, H.A. Padmore, S. Anders, T. Stammler, M.R. Scheinfein, Surf. Rev. Lett. 5 (1998) 1297.
[44] K. Janischowsky, M. Stammler, L. Ley, Diam. Relat. Mater. 8 (1999) 179.
[45] K. Janischosky, M. Stammler, R. Stöckel, L. Ley, App. Phys. Lett. 75 (1999) 2094.

[46] P. Grogger, F. Warbichler, T. Hofer, W. Lang, W. Schintlmeister, Electron Microscopy, in: H.A. Calderon-Benavides, M. Jose-Yacaman (Eds.), 1998 Int. Cong. Electron Microscopy, Cancun, Mexico, Institute of Physics, Bristol, 1998, p. 215.

[47] W. Grahneis, Ch. Ziethen, G.H. Fecher, G. Schönhense, in: Proc. 2nd Int. Conf. Synchrotron, Radiation in Materials Science (SRMS-2), JJAP Supplement 38-1, 1999, ISSN 0021-4922.